SECOND-MOMENT CLOSURE STUDY ON COMBINED EFFECTS OF EXPANSION RATIO AND SWIRL INTENSITY ON TURBULENT MIXING IN MODEL COMBUSTORS

S. Jakirlić, R. Jester-Zürker and C. Tropea
Chair of Fluid Mechanics and Aerodynamics,
Darmstadt University of Technology
Petersenstr. 30, D-64287 Darmstadt, Germany
s.jakirlic@sla.tu-darmstadt.de, roland@sla.tu-darmstadt.de, ctropea@sla.tu-darmstadt.de

ABSTRACT

An isothermal, incompressible, swirling flow in three generic combustor configurations featuring different inflow structure with respect to the circumferential velocity type (both configurations with annular and central swirling jet were considered), combustor confinement (in terms of expansion ratio ER) and swirl intensity (S) was studied computationally by means of Reynolds Averaged Navier-Stokes method (RANS), using Second-Moment Closure (SMC) models. The work focuses on the investigation of the combined effects of the above-mentioned flow parameters on the mixing between a swirling annular jet (representing air stream) and the non-swirling inner jet (representing fuel) within a combustor. Both the basic high-Reynolds number SMC model, modified to account for the non-linearities in the pressure scrambling and dissipation processes, and a low-Reynolds number SMC model, accounting separately for the viscous and non-viscous wall blockage, were applied. Inflow conditions are computationally generated, rather than prescribed. In the course of the inflow data generation, a number of the "equilibrium" swirling flows in the concentric annulus and pipe geometries, from which coaxial and central swirling jets expand into a combustion chamber, are computed. The SMC results reproduced all important mean flow and turbulent features in good agreement with available experimental and LES data.

INTRODUCTION

A technique traditionally used for flame stabilization in a combustor is recirculation of the core flow. The recirculation is a consequence of high angular momentum being confined in the combustor configuration. The appearance of a swirl-induced bubble represents a transition from the non-swirling (or weakly swirling), supercritical flow situation, to the subcritical flow state exhibiting reverse flow in the core. This abrupt change of the flow structure corresponds to the well-known *vortex breakdown* phenomena (see, e.g., Escudier and Keller, 1985). In practically relevant combustion chamber geometries, a non-recirculating flow is established downstream, suggesting that the flow in the combustor is only locally subcritical. This effect is even more pronounced if the flow in combustor is reactive. An increase of the fluid viscosity due to combustion can cause flow acceleration in the streamwise direction, contributing significantly to the re-establishment of the supercritical flow situation. The adverse pressure gradient, being an outcome of the sudden expansion, augments the formation of a free recirculation zone. The combined effects of the enhanced irrotational straining due to bulk flow deceleration (adverse pressure gradient) and local acceleration (in the mixing layer region between the corner bubble and the free recirculation zone), as well as additional straining due to presence of the swirl motion (secondary shearing and streamline curvature effects), cause a weakening of the stress anisotropy, being especially pronounced in the flow core, Jakirlić et al. (2002). Furthermore, it is well known that the swirl motion promotes scalar transport i.e. turbulent mixing. The most important prerequisite, as far as reacting flows are concerned, is to model accurately the scalar mixing.

In the present work, several data sets have been examined which are particularly well suited for assessing the performances of mixing models. These cases include those configurations investigated experimentally by Roback and Johnson (1983), So et al. (1984) and Nejad et al. (1989). In addition to the mean flow and turbulence fields, the first two investigations. provide also results for mean scalar (mixture fraction), scalar variance and scalar fluxes. Moreover, the Roback and Johnson's experimental data base was recently supplemented by the LES results of Pierce and Moin (1998a). The corresponding Reynolds numbers, expansion ratios and swirl intensities are given in Table 1. The Reynolds numbers are related to the incoming bulk flow. All three flow configurations are presented schematically in Fig. 1, illustrating clearly the differences in the structure of swirling inflow. The variability in the inflow conditions increases significantly the sensitivity of the prediction to the quality of the turbulence models.

Test case	Re_S	ER	S	Grid size, CV's High-Re/Low-Re
Roback & Johnson	47.500	2.1	0.41	$200x70/210x120$
So et al.	83.000	1.0	2.24	$250x70/300x130$
Nejad et al.	125.000	1.5	0.5	$240x70/280x120$

Table 1: Characteristics of the flow configurations considered and sizes of the numerical grid used for high and low-Reynolds number model computations

COMPUTATIONAL METHOD

The combustor flows considered are in fact three-dimensional, for which all three velocity components and all six Reynolds stress components must be accounted for. However, the Reynolds-averaged continuity, momentum and concentration equations are solved with assumption of ax-

isymmetry ($\partial/\partial\varphi = 0$):

$$\frac{1}{r}\frac{\partial(rU_j)}{\partial x_j} = 0 \tag{1}$$

$$\frac{1}{r}\frac{\partial(rU_jU_i)}{\partial x_j} = \frac{1}{r}\frac{\partial}{\partial x_j}\left[r\left(\nu\frac{\partial U_i}{\partial x_j} - \overline{u_iu_j}\right)\right] - \frac{1}{\rho}\frac{\partial P}{\partial x_i} + S_{U_i} \tag{2}$$

$$\frac{1}{r}\frac{\partial(rU_jF)}{\partial x_j} = \frac{1}{r}\frac{\partial}{\partial x_j}\left[r\left(\frac{\nu}{Sc}\frac{\partial F}{\partial x_j} - \overline{u_jf}\right)\right] \tag{3}$$

where the vector $x_i(r,z)$ denotes the coordinate directions and $U_i(U_r, U_\varphi, U_z)$ ($\equiv (V,W,U)$) stands for the mean velocity vector. The source terms S_{U_i} arise from the coordinate transformation (see e.g., Jakirlic et al., 2000, for further details about the governing equations written in the cylindrical coordinate frame).

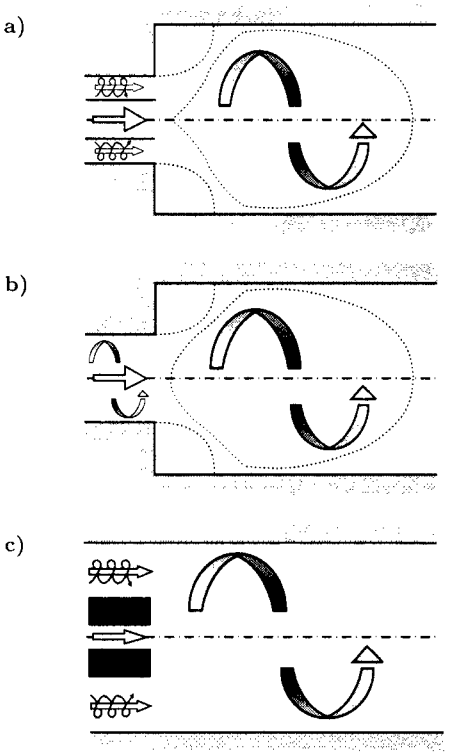

Figure 1: Schematic of the flow cases investigated: a) Roback and Johnson's, b) Nejad's et al. and c) So's et al. model combustors

Numerical framework

All computations were performed by a computer code based on a finite-volume numerical method for solving the Reynolds Averaged Navier-Stokes (RANS) equations in orthogonal coordinate systems with a collocated variable arrangement. The velocity-pressure coupling is achieved by the pressure correction method based on the well known SIMPLE algorithm. The equations are linearized and solved sequentially using an iterative ILU method. Diffusion fluxes are approximated by central differences (CD). For discretization of the convective fluxes, a blended upwind-central differencing scheme, implemented in the so-called deferred-correction manner was used. The value of the blending factor was typically between 0.7 (for Second-Moment Closure models) and 1.0 (for $k-\varepsilon$ models) for all variables. The solution domain typically has the shape of suddenly expanding, axisymmetric pipe geometry, with a length L and a height $R = D/2$, D being the combustor diameter. The final sizes of numerical grid for high and low-Reynolds number model computations are given in Table 1. Other grids, coarser, but also refined, were also used in the course of the grid independence study. The grids were squeezed in the shear layer and near-wall regions, providing the dimensionless wall distance y^+ of the numerical node closest to the wall being approx. 15, when using high-Reynolds models, and less than 0.5, if low-Re models were applied. Standard wall functions were used for high-Reynolds number model computations. It is common to compute combustor flows in a steady manner, if RANS models are used to describe turbulence. The so-called "temporal underelaxation" was applied here to strenghten additionally the diagonal dominance of the coefficient matrix, implying actually the unsteady computations were performed. However, such an unsteady calculation ended up, as expected, in a steady solution.

Turbulence models

Computations were performed with the low-Re-number Reynolds-stress model (Hanjalic and Jakirlic - HJ low-Re SMC, 1998) and with the basic high-Re-number Reynolds-stress model (Gibson and Launder - GLm, 1978) modified to account for the non-linearities in:

- the slow part of the pressure scrambling process, $\Phi_{ij,1}$ (Speziale et al., 1991) and
- the dissipation correlation, ε_{ij} (Hallbäck et al. - HGJ, 1990).

The non-linear parts of the model formulations for $\Phi_{ij,1}$ and ε_{ij} can be easily coupled as follows:

$$\begin{aligned}\Phi_{ij,1} - \varepsilon_{ij} &= -C_1\varepsilon a_{ij} - (C_1' + \alpha)\varepsilon\left(a_{ik}a_{kj} - \frac{1}{3}A_2\delta_{ij}\right) \\ &\quad - \left[(1-f_s)\frac{2}{3}\delta_{ij}\varepsilon + f_s\frac{\overline{u_iu_j}}{k}\varepsilon\right]\end{aligned} \tag{4}$$

where a_{ij} ($= \overline{u_iu_j}/k - 2/3\delta_{ij}$) represents the Reynolds stress anisotropy tensor, A_2 ($= a_{ij}a_{ji}$) its second invariant, $f_s = 1 + \alpha(A_2/2 - 2/3)$ and $\alpha = 3/4$. This most general model for the slow part is quadratic, because the Cayley-Hamilton theorem allows higher powers of a_{ij} to be expressed in terms of a_{ij} and a_{ij}^2. The DNS database for fully developed channel flow enables the evaluation of the profiles of the model coefficients C_1 and C_1'. The coefficient C_1 reaches the standard high-Reynolds number value 1.7 – 1.8 away from the wall (not shown here), in good agreement with most of the existing model proposals.

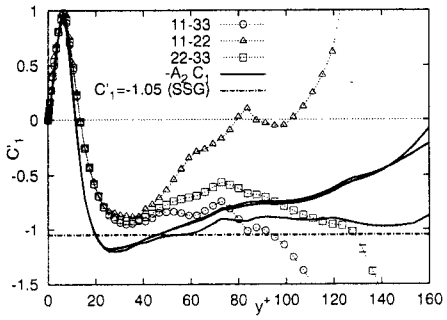

Figure 2: Model coefficient C_1' in the non-linear part of the slow term $\Phi_{ij,1}$ (Eq. 4) deduced from the DNS database of the fully-developed channel flow

The evaluated coefficient C_1' is negative, apart from very close to the wall, exhibiting the opposite behaviour than C_1.

Far from the wall the value of C_1' is close to that proposed by Speziale et al. (1991), $C_1' = -1.05$, at least in the logarithmic region. Here a variable model coefficient in terms of A_2: $C_1' = -A_2 C_1$, in close agreement with the DNS data (Fig. 2), was adopted, (see Hanjalic and Jakirlic, 2002, for more detils).

The HGJ model is developed for homogeneous flows, meaning that the dissipation rate ε actually represents the homogeneous dissipation, which differs from the total dissipation rate only very close to the solid walls ($y^+ \leq 15 - 20$). The non-linear model formulation by Hallbäck et al. captured the dissipation anisotropy, in good agreement with the DNS data of the flows being affected by separation (Fig. 3) and swirling effects (not shown here). The most widely used (isotropic) model of Rotta ($\varepsilon_{ij} = 2/3\delta_{ij}\varepsilon$) is also shown for comparison. It is clearly seen, that the anisotropies of the dissipation correlation are not only pronounced in the immediate wall vicinity, but they also affect the core flow (e.g. mixing layer). This feature is beyond the reach of the Rotta's ansatz.

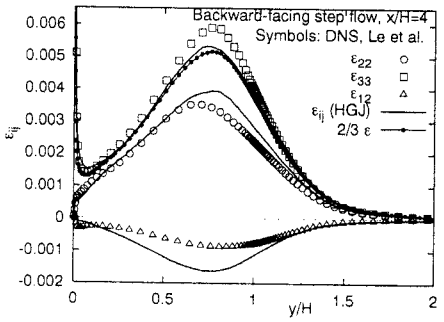

Figure 3: Dissipation correlation components obtained by the HGJ model within the recirculation bubble in the flow over a backward-facing step

It is very well known that the strong swirl causes an enhanced deviation from the 'equilibrium' assumptions, the fact being especially pronounced in the near-wall regions. Therefore a low-Reynolds model, e.g. the HJ low-Re SMC model, should be applied. This was done for the computations of some test cases, e.g. So et al.. However, correct simulation of the near-wall effects (viscosity effects and kinematic wall blocking) has been proven to not be of decisive importance here (see Figs. 7 and 9, where the results of the HJ low-Re SMC model show no significant difference compared to the GLm high-Re model results). This is because of the fairly high bulk Reynolds numbers (see Table 1) and because the most crucial mean flow and turbulence characteristics (flow reversal and mixing) are concentrated in the combustor core and are not influenced by the wall proximity effects in such an isothermal flow situation. Therefore, the HJ low-Re SMC model was only used for the generation of the inflow conditions (see next section).

To account for the effect of the mean flow and turbulence fields on the transport of a passive scalar, that is the concentration (mixture) field F, the Second-Moment Closure model for turbulent scalar transport proposed by Gibson and Launder (1978) and subsequently by Launder and Samaraweera (1979) was adopted. The term in the equation governing the scalar flux $\overline{u_j f}$, corresponding to the pressure-scalar gradient correlation, is modelled in analogy to the linear pressure-strain model in the equation for the Reynolds-stress tensor:

$$\Phi_{if,1} = -C_{1f}\frac{\overline{u_i f}}{\tau};\quad \Phi_{if,2} = C_{2f}\overline{u_k f}\frac{\partial U_i}{\partial x_k} \qquad (5)$$

This model version (denoted as GL/I: $C_{1f} = 3.0$, $C_{2f} = 0.5$) presumes the absence of turbulence interaction with the mean concentration gradient. The characteristic time scale τ is taken to be equal to the scalar time scale of the turbulent velocity field k/ε. Another model variant of the rapid part $\Phi_{if,2}$ including the complete production due to the actions of both mean flow field deformations (velocity and concentration): $P_{if} = -\overline{u_k f}\partial U_i/\partial x_k - \overline{u_i u_k}\partial F/\partial x_k$ was also applied. In this version (denoted as GL/II) the contributions of the mean gradients are split (Jones, 1992), making the model more flexible:

$$\Phi_{if,1} = -C_{1f}\frac{1}{R_\tau}\frac{\overline{u_i f}}{\tau};\quad \Phi_{if,2} = C_{2f}\overline{u_k f}\frac{\partial U_i}{\partial x_k} + C_{3f}ka_{ik}\frac{\partial F}{\partial x_k} \qquad (6)$$

with $R_\tau = 0.8$ and $C_{3f} = 0.25$. Both model variants used here are derived for high Reynolds number, convection dominated (high Peclet number) flows. If flows with low Reynolds and Peclet numbers are to be computed, the models must be modified correspondingly. This is usually done by expressing the model coeficients in terms of the turbulence Reynolds and Prandtl numbers, accounting also for a more suitable time scale τ, which should include the scalar variance $\overline{f^2}$ and its dissipation rate ε_f (see e.g. the works of Shikazono and Kasagi, 1996, and Kawamura and Kurihara, 2000). The inclusion of the coefficient R_τ, representing actually the ratio of the time scales $((\overline{f^2}/\varepsilon_f)/(k/\varepsilon))$, accounts for such conditions (Rodi, 1980).

In addition, all flow cases considered are solved using the standard high-Reynolds number $k-\varepsilon$ model and its low-Reynolds number extension due to Launder and Sharma (1974).

Inflow conditions

The specification of the inflow boundary conditions in the case of swirling flows deserves special attention. The inlet cross-section of the computational domain typically coincides with the first available measurement location, usually being situated in the interior of the combustor. In this work the inlet boundary was located prior to the expansion and the inflow data were generated by performing a separate computation of the fully developed, annular, swirling flow, imposing a uniform profile of the fictitious azimuthal pressure gradient (azimuthal body force), in accordance with the proposal of Pierce and Moin (1998b). Fig. 4 shows the mean circumferential velocity W and corresponding turbulent shear stress components $\overline{uw}$ and $\overline{vw}$ across the concentric annulus of the Roback and Johnson's model combustor obtained by such a computational procedure.

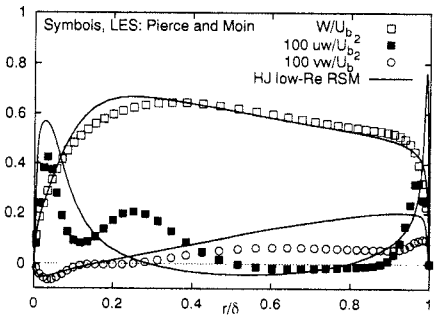

Figure 4: Mean velocity and shear stress profiles across the annular swirling flow of the Roback and Johnson's combustor configuration

The low-Reynolds number Second-Moment closure model due to Hanjalic and Jakirlic (1998), tested in a range of the flow situations featuring different mean flow and turbulent phenomena, was used for the inflow data generation. Correct capturing of the highly anisotropic near-wall region of the fluid streams in the concentric annulus and central pipe was very important, keeping in mind that these wall layers unify in the combustor, transforming into a curved shear layer.

Locating the inlet cross-section of the solution domain prior to the expansion is especially important if the scalar transport is to be accounted for. In such a way the inlet conditions for the concentration and scalar fluxes are related to the annular and inner streams (zero scalar fluxes) prior to their mixing.

RESULTS AND DISCUSSION

Fig. 5 upper displays the streamline pattern obtained by the GLm model illustrating clearly the mean flow structure, being characterized by an annular recirculation region (corner bubble) and a large free separation region in the core flow.

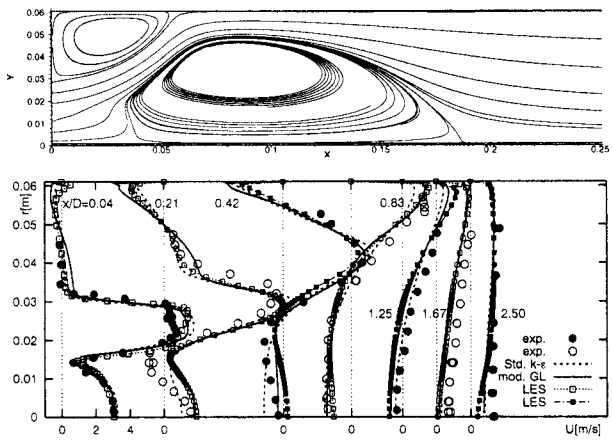

Figure 5: Computationally (by using the modified GL SMC model) obtained streamline pattern (upper) and evolution of the mean axial velocities (lower) in the Roback and Johnson's combustor configuration ($D = 122mm$)

A short wake region between the inner and annular streams passes into a large-eddy shear region between both recirculation zones. The most intensive turbulence production, and finally mixing, occurs just in this flow region bordering both the central and corner bubbles. Whereas the annular swirling jet separates at the sharp edge of the sudden expansion, generating the corner bubble, both the separation and reattachment points of the large recirculation zone are situated on the combustor centerline i.e. in the free stream. Proper prediction of the separation onset and reattaching length of such a free bubble represents a special challenge for statistical turbulence models. Figs. 5 lower, 6 lower and 7 upper show the evolution of the mean axial velocity profiles for all three model combustors investigated. Whereas the joint effects of the high expansion ratio ($ER = 2.1$) and strong swirling inflow in the case of the Roback and Johnson's combustor were suprisingly well predicted by the standard $k - \varepsilon$ model, Fig. 5 lower (in spite of the inherent, well-known weaknesses of treating swirl and separation separately), the somewhat milder flow expansion ($ER = 1.5$, Nejad et al. case), by comparable swirl intensity (see Table 1) was very poorly predicted. The free separation zone was totally missed using the standard $k - \varepsilon$ model, Fig. 6 lower. Both the shape of the free separation zone and its length are correctly predicted by the GLm model described above, Figs. 6.

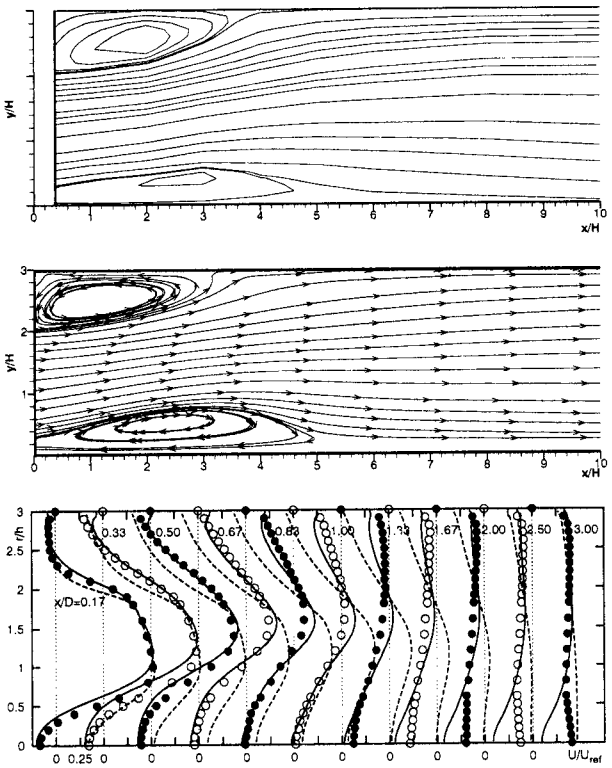

Figure 6: Experimentally (upper) and computationally (middle) obtained (by using the modified GL SMC model) streamline patterns (middle) and evolution of the mean axial velocities (lower) in the Nejad's et al. ($D = 152,4mm$, $H = 50,8mm$) combustor configuration. Key as Fig. 5

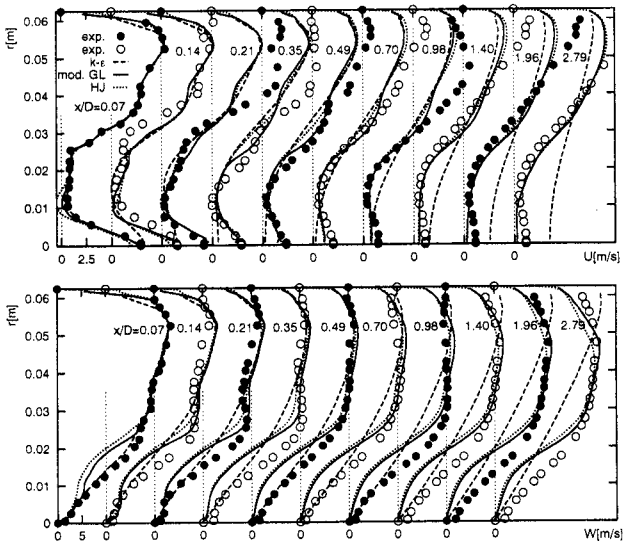

Figure 7: Evolution of the mean axial (upper) and mean circumferential (lower) velocities in the So's et al. combustor configuration

Although no free separation occurs in the third flow configuration (due to a small, non-swirling central jet)

examined by So et al., a similar misrepresentation of the axial flow using the standard, linear $k-\varepsilon$ model is observed, Fig. 7 upper. Another consequence of isotropic eddy viscosity is the so-called "solid-body rotation" form of the tangential velocity profile, Fig. 7 lower, which is always obtained, independent of the initial velocity profile. One of the reasons for such a behaviour is the simple linear relationship between Reynolds-stress and mean rate of strain tensors, implying essentially that the eddy viscosity is isotropic. But it is well known that swirl causes a strong anisotropy of both the stress and dissipation tensors, as well as a highly anisotropic eddy viscosity. Fig. 8 displays the evolution of the streamwise turbulence intensity and the shear stress component in the Roback and Johnson's flow.

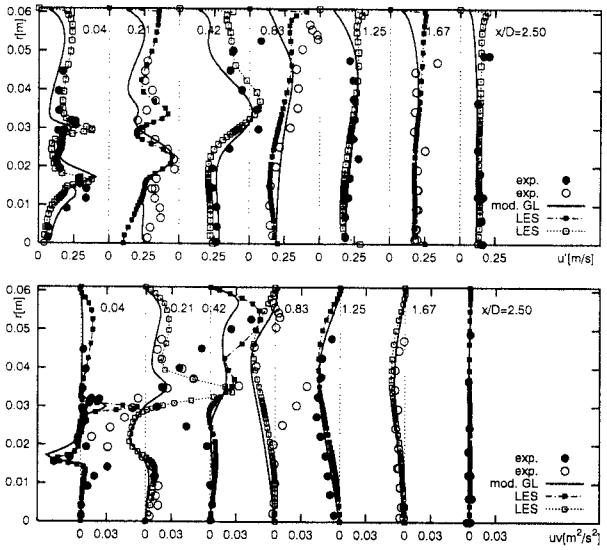

Figure 8: Evolution of the streamwise turbulence intensity (upper) and the shear stress component (lower) in the Roback and Johnson's combustor configuration

The highest values of this turbulence quantity are clearly located in the regions of the strong mean shear, where the most intensive interaction between the mean and reversed flow regions and turbulence takes place. Both phenomena, the separation due to sudden expansion and strong swirl in the entrance region, are associated with the adverse pressure gradient effects, which, as already known, promote an isotropic state (see also Fig. 9). It leads to the weakening of the stress anisotropy, which is most pronounced in the combustor core. Such a behaviour is closely connected to the creation of a large, free recirculation zone. The profiles of the other diagonal stress components (not shown here) are similarly shaped. The shear stresses are somewhat underpredicted in regions coinciding with the shear layers, reflecting the well-known weakness of statistical turbulence models. Fig. 9 shows the streamwise and spanwise Reynolds stress components at selected locations in the So's et al. combustor indicating their enhanced production rate around the combustor center in the entrance region, being the consequence of the strong secondary shearing ($\partial W/\partial r$) and streamline curvature effects ($-W/r$), but also the tendency towards isotropic state.

Figs. 10 show some results - the evolution of the mixture fraction F and the streamwise ($\overline{uf}$) scalar flux component in the Roback and Johnson's model combustor - obtained by using the Second-Moment closure model for the scalar transport.

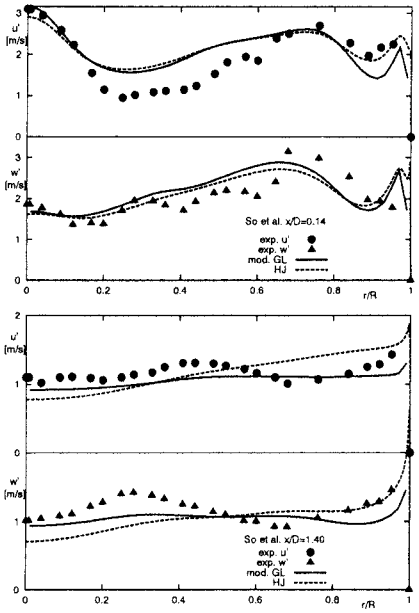

Figure 9: Streamwise and spanwise Reynolds stress component at selected locations in the near (upper) and far (lower) field of the So's et al. combustor configuration

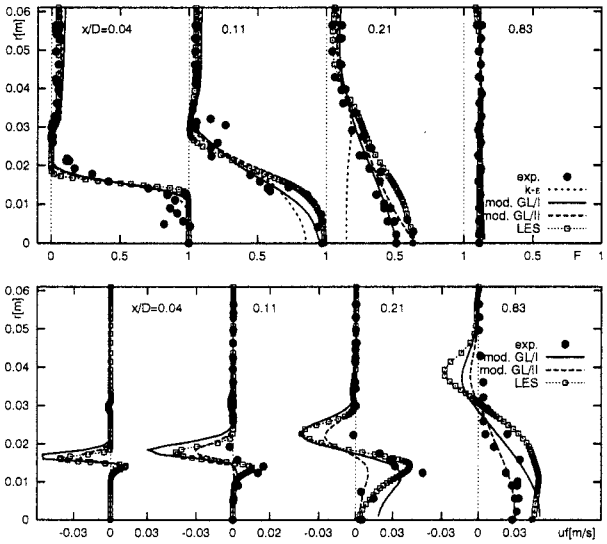

Figure 10: Profiles of the mixture fraction F and the streamwise scalar flux $\overline{uf}$ at selected locations for the Roback and Johnson case

The change in profiles of F indicate a rapid spreading of the central stream i.e. very intensive mixing, which is completed already after three step heights ($x/D = 0.83$). This corresponds roughly to the middle of the central recirculation zone. Contrary to the SMC computations, the $k-\varepsilon$ model results in a completely uniform profile already at the position $x/D = 0.21$. Keeping in mind very good agreement of the mean velocities obtained by both model groups with the experimental and LES results, the reason for this deviation can only lie in the isotropic nature of the gradient diffusion hypothesis being exploited in the $k-\varepsilon$ model scheme. The SMC calculations result in a high negative value of the scalar flux $\overline{uf}$ in the mixing layer between non-swirling central and swirling annular jets, agreeing well with the LES data. It is interesting to note that such a negative

value was not detected by the measurements. Both sets of the SMC-results, with (GL/II) and without (GL/I) the contribution of the mean concentration gradient in the rapid part of the redistribution term, are presented. It should be noted that this gradient contributes to this process only in the flow regions, where the Reynolds-stress anisotropy exists (Eq. 6). Whereas this addition acts as a sink in the flow core (where a strong negative streamwise gradient of F occurs: $a_{11}\partial F/\partial x < 0$), its influence acts towards the reduction of the negative value of $\overline{uf}$ (actually its source) in the surrounding mixing layer ($a_{12}\partial F/\partial r > 0$). The modification of the slow part through inclusion of the coefficient R_τ, accounting for difference in the time scales (see chapter 2.2), contributes even stronger to the behaviour described. Its influence depends on the sign of the stress flux $\overline{uf}$. This term acts as a source in the regions with negative $\overline{uf}$ (shear layer), and, it causes a reduction of $\overline{uf}$ if the stress flux $\overline{uf}$ itself takes a positive value.

CONCLUSIONS

Three swirling flow configurations akin to those encountered in combustion chambers were numerically investigated. The variability in the inflow conditions significantly influences the prediction results, depending on the turbulence models used. Second-moment closure models, providing information about all stress components and containing exact generation terms for dealing with the swirling i.e. strong streamline curvature effects in the Reynolds-stress and scalar flux transport equations, are inherently capable of capturing most of the phenomena mentioned. Indeed, in contrast to the k-ε models, in all flow cases reported here the second-moment closures produced superior results.

Acknowledgements

This work has been financially supported by the Deutsche Forschungsgemeinschaft (DFG) through the grant SFB 568. The authors thank Prof. Parviz Moin and Dr. Charles Pierce for making available their LES results of the Roback and Johnston's combustor. We are especially indebted to Charles Pierce, who, at the very end of 2001, managed to extract the mean statistics of the LES body of data (not published) for our investigations inspite of his serious illnes. He passed away only a few months later.

REFERENCES

Eggels, J.G.M., Boersma, B.J., and Nieuwstadt, F.T.M. (1994): Direct and Large-Eddy Simulations of Turbulent Flow in an Axially Rotating Pipe. Lab. for Aero- und Hydrodynamics, Delft University of Technology, Delft, The Netherlands, October

Escudier, M.P., and Keller, J.J. (1985): Recirculation in Swirling Flow: A Manifestation of Vortex Breakdown. *AIAA J.*, Vol. **23**, No. **1**, pp 111-116

Gibson, M.M., and Launder, B.E. (1978): Grounds Effects on Pressure Fluctuations in the Atmospheric Boundary Layer. *J. Fluid Mech.*, Vol. **86**, pp. 491-511

Hallbäck, M., Groth, J., and Johansson, A.V. (1990): An algebraic model for nonisotropic turbulent dissipation rate in Reynolds stress closures. *Physics of Fluids A2*, Vol. **10**, pp. 1859-1866

Hanjalić, K., and Jakirlić, S. (1998): Contribution towards the second-moment closure modelling of separating turbulent flows. *Computers and Fluids*, Vol. **27**, pp. 137-156

Hanjalić, K., and Jakirlić, S. (2002): Second-Moment Turbulence Closure Modelling. In *Closure Strategies for Turbulent and Transitional Flows*, B.E. Launder and N.H. Sandham (Eds.), Cambridge University Press, Cambridge, UK, pp. 47-101

Jakirlić, S., Volkert, J., Pascal, H., Hanjalić, K., and Tropea, C. (2000): DNS, experimental and modelling study of axially compressed in-cylinder swirling flow. *Int. J. of Heat and Fluid Flow*, Vol. **21**, No. **5**, pp. 627-639

Jakirlić, S., Hanjalić, K., and Tropea, C. (2002): Modelling Rotating and Swirling Flows: A Perpetual Challenge. *AIAA J.*, Vol. **40**, No. **10**, pp 1984-1996

Kawamura, H, and Kurihara, Y. (2000): Modelling of turbulent scalar transport in homogeneous turbulence. *Int. J. Heat and Mass Transfer*, Vol. **43**, pp. 1935-1945

Jones, W.P. (1992): Turbulence modelling for combustion flows. In *Modelling for combustion and turbulence*, Lecture Series 1992-03, von Karman Institute for Fluid Dynamics

Launder, B.E., and Sharma, B.I. (1974): Application of the Energy-Dissipation Model of Turbulence to the Calculation of Flow Near a Spinning Disc. *Letters in Heat and Mass Transfer*, Vol **1**, pp. 131-138

Launder, B.E., and Samaraweera, D.S.A. (1979): Application of a Second-Moment Turbulence Closure to Heat and Mass Transport in Thin Shear Flows - I. Two-Dimensional Transport. *Int. J. Heat and Mass Transfer*, Vol. **22**, pp. 1631-1643

Le, H., Moin, P., and Kim, J. (1997): Direct numerical simulation of turbulent flow over a backward-facing step. *J. Fluid Mech.*, Vol. **330**, pp. 349-374

Nejad., A.S., Vanka, S.P., Favaloro, S.C., Samimy, M. and Langenfeld, C. (1989): Application of Laser Velocimetry for Characterization of Confined Swirling Flow. *ASME J. Eng. for Gas Turbines and Power*, Vol. **111**, pp. 36-45

Pierce, C.D., and Moin, P. (1998a): LES of a confined coaxial jet with swirl and heat release. *AIAA Paper* 98-2892

Pierce, C.D., and Moin, P. (1998b): Method for Generating Equilibrium Swirling Inflow Conditions. *AIAA J.*, Vol. **36**, No. **7**, pp. 1325-1327

Roback, R., and Johnson, B.V. (1983): Mass and Momentum Turbulent Transport Experiments with Confined Swirling Coaxial Jets. NASA Contractor Report 168252

Rodi, W. (1980): Turbulence models for environmental problems. In *Prediction Methods for Turbulent Flows*, W. Kollmann (Ed.), von Karman Institute for Fluid Dynamics pp. 259-349

Shikazono, N., and Kasagi, N. (1996): Second-moment closure for turbulent scalar transport at various Prandtl numbers. *Int. J. Heat and Mass Transfer*, Vol. **39**, No. **4**, pp. 2977-2987

So, R.M., Ahmed, S.A., and Mongia, H.C. (1984): An Experimental Investigation of Gas Jets in Confined Swirling Air Flow. NASA Contractor Report 3832

Speziale, C.G., Sarkar, S., and Gatski, T.B. (1991): Modelling the Pressure-Strain Correlation of Turbulence: an Invariant Dynamical Systems Approach, *J. Fluid Mech.*, Vol. **227**, pp. 245-272